Journal of Materials Chemistry A

PAPER

View Article Online
View Journal | View Issue

Cite this: J. Mater. Chem. A, 2014, 2, 15611

A facile one-step synthesis of three-dimensionally ordered macroporous N-doped TiO_2 with ethanediamine as the nitrogen source

Ting Wang,[a] Xiaoqing Yan,[a] Shishun Zhao,[a] Bo Lin,[a] Chao Xue,[a] Guidong Yang,*[a] Shujiang Ding,[b] Bolun Yang,[a] Chuansheng Ma,[c] Guang Yang[c] and Guorui Yang[d]

Received 18th April 2014
Accepted 16th July 2014

DOI: 10.1039/c4ta01922a

www.rsc.org/MaterialsA

In this paper, three-dimensionally ordered macroporous (3DOM) N-doped anatase TiO_2 (N-TiO_2) photocatalysts with well-defined macroporous skeletons were prepared using a simple one-step colloidal crystal-templating method. Organic ammonia ethanediamine was used as the nitrogen source during preparation to enhance nitrogen incorporation into the TiO_2 lattice. The photocatalytic performance of the as-prepared 3DOM N-TiO_2 was investigated by measuring the degradation of rhodamine B (RhB) and the generation of H_2 from water splitting under simulated visible-light conditions. In comparison with the pure TiO_2 and N-doped TiO_2, the results of photodegradation and photocatalytic hydrogen generation reactions showed that the 3DOM N-TiO_2 sample exhibited excellent catalytic activity under visible-light irradiation. In addition, various analytical techniques have been used to characterize the crystal phase, morphology and optical absorption of the obtained samples. The results showed that the 3DOM N-TiO_2 catalyst was successfully synthesized by the one-step colloidal crystal-templating method, and the as-prepared samples possessed well-defined 3DOM skeleton structure, high crystallinity and enhanced visible-light-driven photocatalytic activities.

Introduction

It is well-known that three-dimensionally ordered macroporous (also known as "inverse opals" or "inverted opals") materials[1] possess uniform pore size, well-defined periodic structure and large surface areas,[2,3] which indicate various potential applications in the fields of battery materials, catalysts or catalyst supports, sensors, biomaterials[4,5] and photonic crystals,[6] and have thus received significant attention. More recently, numerous studies have focused on the fabrication of 3DOM materials by a variety of synthetic routes. In particular, the colloidal crystal-templating method with polymethyl methacrylate (PMMA), monodisperse silica, or polystyrene (PS) spheres as templating agent has received significant attention because of its low cost and high repeatability.[1] To date, advances have been made in preparing 3DOM-structured materials (*e.g.*, 3DOM-structured C,[7] MnO_2,[8] Mn_2O_3, Fe_2O_3, Co_3O_4, NiO, CuO,[9] and PbO_2 (ref. 10)).

As a class of important semiconductor materials, porous TiO_2 catalysts have attracted increasing interest because of its unique optoelectronic and physiochemical properties, particularly for TiO_2 with 3DOM structure, which has been become a hotspot in the field of porous materials because of its several merits in photocatalysis, including ordered and uniform macroporous structure, large surface area, improved mass transfer properties and high light-absorption efficiency, caused by multiple scattering and slow photons.[11] In addition, these previously mentioned advantages could efficiently lead to the enhancement of photocatalytic activity of 3DOM TiO_2.[12] However, the relatively broad band gap of 3DOM anatase titania (3.2 eV) and the rapid recombination of photogenerated electron–hole pairs limit its large-scale applications.[13,14] To overcome the drawbacks and improve photocatalytic activity, significant efforts have been made to explore various strategies (*e.g.* doping with anion[15–17] and combing with narrow band gap semiconductor[18–20]) to modify the TiO_2 photocatalyst. Among these strategies, nonmetal doping has been frequently applied for achieving visible-light-active TiO_2 photocatalysts, particularly TiO_2 with nitrogen doping, which have been extensively investigated during the past decades. Such doping could not only effectively modify the TiO_2 energy band gap and accelerate electron–hole separation but could also lead to an apparent redshift in the optical absorption edge of TiO_2 to lower energy,

[a]Department of Chemical Engineering, School of Chemical Engineering and Technology, Xi'an Jiaotong University, Xi'an, 710049, China. E-mail: guidongyang@mail.xjtu.edu.cn; Fax: +86-29-8266-3189

[b]Department of Applied Chemistry, School of Science, Xi'an Jiaotong University, Xi'an, 710049, China

[c]Electronic Materials Research Laboratory, Key Laboratory of the Ministry of Education, Center for Dielectric Research, Xi'an Jiaotong University, Xi'an 710049, China

[d]Department of Environmental Science & Engineering, Xi'an Jiaotong University, Xi'an 710049, China

resulting in a significant improvement of photocatalytic activity under visible light. Until now, a variety of nitrogen sources, including urea,[21] guanidine carbonate,[22] ammonium hydroxide[23] and ethanediamine,[24] have been explored to synthesize TiO_2 nanocrystals with N-doping. Among these nitrogen precursors, ethanediamine, a special organic nitrogen source, was considered to be an excellent nitrogen-containing species for preparing the N-doped TiO_2 photocatalyst because ethanediamine can be easily dissolved in water or ethyl alcohol. Therefore, nitrogen species can be uniformly and effectually introduced into the anatase TiO_2 crystalline structure. Thus far, very little work has been reported on the preparation of 3DOM TiO_2 materials with N doping. Moreover, the complicated preparation process, which requires at least two or three steps, further limits the use of N-doped TiO_2 with 3DOM structure.

In this paper, a simple yet efficient one-step colloidal crystal-template method was developed to synthesize N-doped TiO_2 with three-dimensionally ordered macroporous structure. Moreover, organic ammonia ethanediamine was used as a nitrogen source to achieve N doping. The as-prepared photocatalysts are characterized by X-ray powder diffraction (XRD), scanning electron microscopy (SEM), energy dispersive X-ray spectrometry (EDX), transmission electron microscopy (TEM), Fourier transform infrared (FT-IR), UV-vis diffuse reflectance spectroscopy (DRS), N_2 adsorption–desorption, and X-ray photoelectron spectroscopy (XPS). The photocatalytic activity of the 3DOM N-TiO_2 was evaluated by the photodegradation of rhodamine B (RhB) and photocatalytic H_2 evolution from water splitting under visible light, which show significantly higher photocatalytic efficiency than the pure N-TiO_2 and TiO_2 nanoparticles.

Experimental

Synthesis of 3DOM N doped TiO_2

PMMA spheres were prepared by modified emulsifier-free emulsion polymerization of MMA, as described elsewhere.[25] 3DOM N-TiO_2 catalysts were synthesized through a one-step colloidal crystal-templating method. Briefly, 0.01 mol of tetrabutyl titanate was dissolved into 30 mL of ethanol solution containing 1 mL of glacial acetic acid under vigorous stirring to form a solution of TiO_2 precursor, and 0.01 mol of ethanediamine was added to the aforementioned TiO_2 precursor solution, accompanied by continuous stirring for 30 min at room temperature to form a mixture solution. 3 g PMMA was then immersed into the mixture and maintained at room temperature overnight to obtain the monolith of the 3DOM N-TiO_2 precursor. Afterward, the monolith was dried at 80 °C overnight and then calcined at 500 °C for 4 h with a ramp rate of 1 °C min^{-1} in a muffle furnace under stationary air to obtain the final 3DOM N-TiO_2 catalyst. For comparison, the N-TiO_2 nanoparticles were synthesized by the same process without the addition of the PMMA template. The pure TiO_2 nanoparticles were also prepared using the aforementioned method without the addition of ethanediamine and the PMMA template.

Characterizations

The crystalline structure and phase component were obtained on an X-ray powder diffractometer (XRD; SHIMADZU, Lab X XRD-6000). The geometry and morphology of the catalyst were acquired by field-emission scanning electron microscopy (JEOL, JSM-6700F), and energy dispersive X-ray spectroscopy (EDX) was employed for elemental analysis. The structure and surface states of photocatalytic composites were obtained through transmission electron microscopy (JEOL, JEM-2100). Fourier transform infrared (FT-IR) spectra (Nicolet Avatar 360) were used to obtain the information regarding functional groups on the surfaces of materials by the potassium bromide tablet method. The optical properties of the samples were detected using a Hitachi U-4100 UV-vis spectrometer in diffuse reflectance mode with $BaSO_4$ as the reflectance. The spectra were recorded at room temperature in the range between 200 nm and 700 nm. N_2 adsorption–desorption isotherms of the samples were collected on an ASAP-3000 BET analyzer to obtain the textural properties of the catalysts. The specific surface area and pore-size distribution plots of the as-prepared samples were calculated by the Brunauer–Emmett–Teller (BET) equation and Barrett–Joyner–Halenda (BJH) method, respectively. The X-ray photoelectron spectroscopy (XPS) was performed on a Kratos AXIS Ultra Dld photoelectron spectrometer with monochromatic Al-Kα excitation ($h\nu$ = 1486.69 eV) and a charge neutralizer to investigate the elemental content and electronic states on the surface of the as-prepared samples. The fitted curves were obtained with XPSPEAK software, and all the bonding energies were calibrated to the C (1s) internal standard peak at 284.8 eV.

Photocatalytic testing

Photocatalytic degradation of RhB. The photocatalytic activities of the as-prepared 3DOM N-TiO_2 catalysts were evaluated by decomposing rhodamine B dye under visible-light irradiation at room temperature. An overhead 300 W xenon lamp (NBeT, HSX-F300, Beijing) equipped with a UV filter (HSX-UV300) was the simulated photosource and was mounted with a 420 nm cut-off glass filter to ensure only visible-light irradiation. The distance between the visible light source and the RhB solution was about 10 cm. In each experiment, 0.07 g as-prepared photocatalyst was added into 70 mL aqueous solution of RhB dye (10 mg L^{-1}) to perform the reaction suspension. Before the photoreaction, the suspension was magnetically stirred in dark for 40 min to establish an adsorption–desorption equilibrium between the catalyst surface and the RhB solution. The solution was then exposed to visible light under continuous magnetic stirring to carry out the photodegradation reaction. During the photoreaction, about 3 mL of the suspension was withdrawn and centrifuged (13 000 rpm for 5 min) to remove catalyst particles every 30 min, and the residual RhB was analyzed by a UV-vis spectrophotometer (UV-1900PPC, Shanghai, China) at 554 nm to obtain its absorbance values. As is known, the concentration of RhB is directly proportional to its absorbance. Hence, the degradation efficiency (x) of RhB can be calculated by the formula $x = C/C_o \times 100\%$, where C_o is the

concentration of the original RhB solution after 40 min adsorption, and C is the concentration of RhB solution after every 30 min reaction. In addition, the photoactivity of the as-prepared samples under full sunlight irradiation was evaluated by the same process previously described, except for the xenon lamp mounted with a 420 nm cut-off glass filter.

To test the stability and reusability of the as-prepared samples, we performed repeated photocatalytic experiments: 0.07 g 3DOM N-TiO_2 was dispersed in 70 mL RhB solution (10 mg L^{-1}), and the procedures of photoreaction were the same as previously described, except the photoreaction time, which was limited to 120 min. After each round of the reaction, the mixture was centrifuged to collect the catalysts. The separated catalyst was then washed and dried for several hours at 80 °C. Afterward, the dried samples were added back to the catalytic reaction system to perform the degradation of RhB under the same conditions.

Photocatalytic H_2 evolution from water splitting. The photocatalytic activities of the as-prepared 3DOM N-TiO_2, N-TiO_2 and TiO_2 nanoparticles were also tested by photocatalytic H_2 evolution under visible-light irradiation. The reaction steps were as follows: 0.05 g as-prepared catalyst was dispersed in a 50 mL aqueous solution consisting of 0.25 M Na_2S and 0.35 M Na_2SO_3, which were used as sacrificial agents to avoid catalytic photocorrosion. Prior to illumination, the system was bubbled with nitrogen for 15 min to ensure that the reaction system was under anaerobic conditions. The amount of H_2 generation was determined through gas chromatography (Agilent Technologies: 6890N) with a thermal conductivity detector (TCD) mounted with a 5 Å molecular sieve using N_2 as the carrier gas.

Results and discussion

3DOM N-doped TiO_2 photocatalysts were prepared by a one-step colloidal crystal-templating method, which was considered to be one of the promising approaches for the fabrication of various types of porous materials. The probable synthesis process is schematically illustrated in Fig. 1. As shown, monodisperse PMMA spheres were first synthesized by a modified emulsifier-free-polymerization method.[25] Moreover, these monodisperse PMMA spheres can easily self-assemble to form orderly colloidal crystal layers under centrifugation. The PMMA colloidal crystal template was then immersed into a precursor solution consisting of tetrabutyl titanate ($Ti(OBu)_4$) and ethanediamine ($C_2H_4N_2H_4$), which were used as titanium and nitrogen sources, respectively. In the initial stages of chemical reaction, tetrabutyl titanate molecules rapidly reacted with ethanediamine to generate the substituted $Ti(OBu)_{4-n}(C_2H_4N_2H_4)_n$ precursor. With an increase in aging time, countless $Ti(OBu)_{4-n}(C_2H_4N_2H_4)_n$ micelles were filled into the interstices of the PMMA blocks and were gradually connected by hydrogen bonding to create an "inverse-opal" structure in three dimensions. The post-treatment of calcinations was followed to obtain the final 3DOM N-doped TiO_2 photocatalysts (a multi-layer porous structure can be clearly seen from the SEM image); this process can effectively remove the PMMA colloidal crystal template and can completely incorporate nitrogen into the lattice of TiO_2. Simultaneously, calcination also leads to the enhancement of the crystalline degree of N-doped TiO_2, resulting in higher visible-light-driven photocatalytic activity. It is noteworthy that the structure of the PMMA template and the immersion process were the key factors to obtain the final N-doped TiO_2 with 3DOM structure. If the structure of the PMMA template was unordered or the immersion process was insufficient, the structure of the final product was not uniform or ordered.

Fig. 2 shows the XRD pattern of 3DOM N-TiO_2 including TiO_2 and N-TiO_2 nanoparticle data used as references. It can be seen that several narrow and sharp peaks located at 2θ values of 25.32°, 37.80°, 48.20°, 53.97°, 55.06°, 62.75°, 68.91°, 70.29°, and 75.07° can be observed in the patterns of all the as-prepared samples, which correspond to the peaks of anatase TiO_2 of (101), (004), (200), (105), (211), (204), (116), (220), and (215) crystal planes (JCPDS: 21-1272), respectively. No other peaks, such as N–O and Ti–N bonds, can be found, indicating that N either doped into the TiO_2 lattice or highly dispersed on the surface of TiO_2, which accords with the other nitrogen-doped TiO_2 reported previously.[24,26,27] In addition, the higher intensity of the main (101) Bragg peak anatase show that these samples possess high crystalline structure.

Fig. 3 shows the SEM images of the self-made PMMA template and the as-prepared 3DOM N-TiO_2 sample, including the data for N-TiO_2 and TiO_2 nanoparticles, which are used here as references. It can be seen from Fig. 3a and b that the N-TiO_2

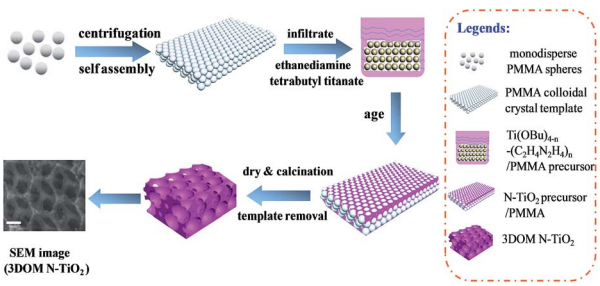

Fig. 1 Schematic synthesis process steps of 3DOM N-TiO_2 sample.

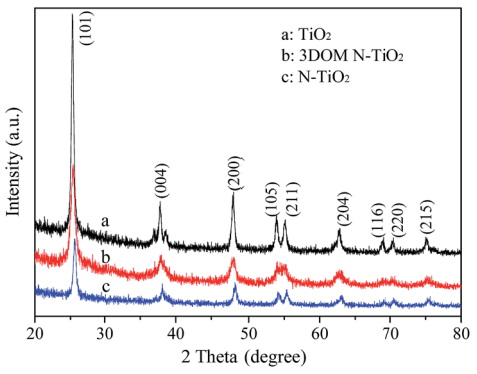

Fig. 2 X-ray diffraction patterns of pure TiO_2, N-TiO_2 and 3DOM N-TiO_2.

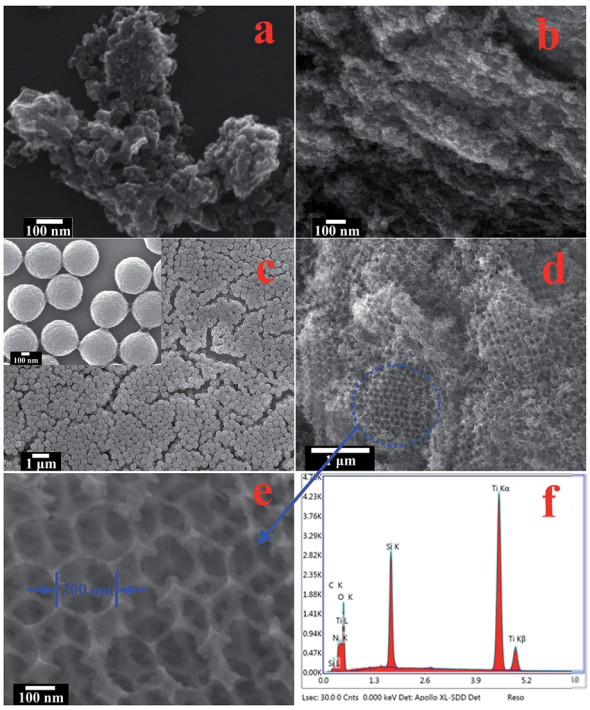

Fig. 3 SEM images of TiO_2 (a); N-TiO_2 (b); PMMA (c); 3DOM N-TiO_2 (d and e); and energy-dispersive X-ray pattern of 3DOM N-TiO_2 (f).

and pure TiO_2 samples present aggregate structures, which are composed of a large quantity of nanoparticles. Fig. 3c clearly shows that the colloidal crystal template contains numerous highly ordered, closely packed spheres. Moreover, the inset of Fig. 3c confirms that the template is prepared from periodic microspheres with a diameter of 350 nm. Fig. 3d shows the low-magnified SEM image of the as-prepared 3DOM N-TiO_2 catalyst. It is apparent that 3DOM N-TiO_2 catalysts display an open, interconnected macroporous network, which is a replication of three-dimensional, closely packed PMMA opals. The opal sizes of photocatalysts are smaller than the size of the original PMMA template particles, which can be attributed to the shrinkage of window size during calcination. However, the well-defined 3DOM framework can be still observed in the sample, indicating the good thermal stability of the samples. Fig. 3e shows the high-magnification SEM image of the N-TiO_2 with 3DOM structure, which clearly showed that the as-prepared N-TiO_2 are 3D-interconnected macroporous networks consisting of periodic spherical voids. It is worth noting that each large pore is connected with six neighboring spheres and circular windows, where the original PMMA spheres contacted with each other. In addition, the origin of the windows was mainly attributed to the fact that the PMMA spheres were so close that the $Ti(OBu)_{4-n}(C_2H_4N_2H_4)_n$ precursor solution did not penetrate those regions.

In addition, Fig. 3f shows the energy-dispersive X-ray results of the 3DOM N-TiO_2. EDX analysis shows that the 3DOM N-TiO_2 catalyst is composed of Ti, O, N, C and Si elements, which confirms the presence of N in the 3DOM N-TiO_2 sample. Carbon (atomic percent of 13.23%) was also observed in the spectra, probably because of the incomplete removal of the PMMA template during calcination, and the EDX signal for Si can be attributed to the utilization of silicon substrate in the SEM testing process.

The typical macroporous structure and crystallization of the 3DOM N-TiO_2 sample were further analyzed by TEM and HRTEM. As shown in Fig. 4a and b, the TiO_2 and N-TiO_2 photocatalysts possess typical nanoparticle morphology with an average grain size of 15–20 nm, which is consistent with the SEM analysis. The insets of Fig. 4a and b are the selected-area electron diffraction patterns of TiO_2 and N-TiO_2, which show clear bright electron diffraction rings, revealing that the reference samples possess good crystallinity, which is in agreement with the XRD analysis. It can be seen from Fig. 4c that the as-obtained 3DOM N-TiO_2 displays well-defined ordered macroporous structure and the formation of the porous skeleton of the catalyst are composed of many nanoparticles with a size of ~10 nm resulting from the aggregation of ultrafine metallic oxide, which is consistent with the SEM results. In addition, the presence of crystal planes and lattice fringes of the 3DOM N-TiO_2 can be clearly observed in the HR-TEM image (Fig. 4d), which were obtained from an individual nanoplate of the pore wall. It further confirms the good crystallinity of the 3DOM N-TiO_2. The reflections with d spacing values of 0.338 nm observed in Fig. 4b are in good agreement with the TiO_2 crystal (204) lattice planes. In addition, the inset of Fig. 4d shows the selected area electron diffraction (SAED) pattern of 3DOM N-TiO_2. A sequence of bright electron diffraction rings can be clearly observed, which confirms the good crystallinity of 3DOM N-TiO_2 which in accordance with the XRD analysis.

Fig. 5 shows the FT-IR spectra of 3DOM N-TiO_2, N-TiO_2 and pure TiO_2 nanoparticles, which provides information regarding functional groups on the surface of catalyst. All the as-prepared samples present similar FT-IR spectra, and the peak in the range of 400–750 cm^{-1} was assigned to the Ti–O stretching and Ti–O–Ti bridging stretching bond. In addition, the absorbance band at 3400 cm^{-1} in the three spectra can be attributed to

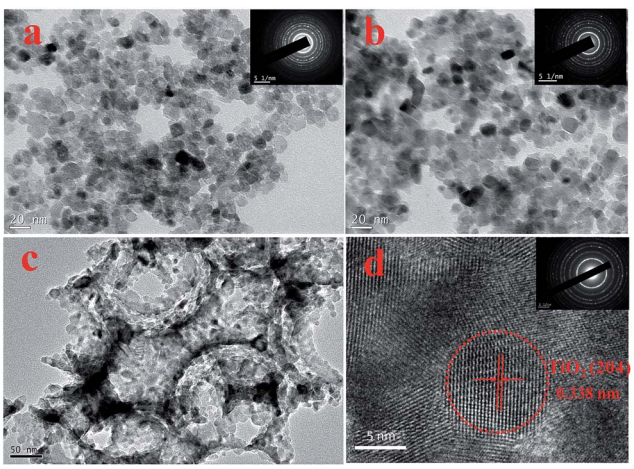

Fig. 4 TEM images of TiO_2 (a); N-TiO_2 (b); 3DOM N-TiO_2 (c); HRTEM image of 3DOM N-TiO_2 (d).

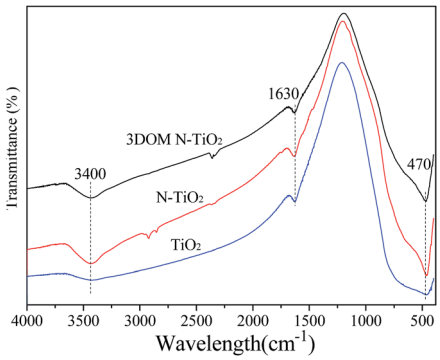

Fig. 5 FT-IR spectra of 3DOM N-TiO_2, N-TiO_2 and pure TiO_2.

surface hydroxyl groups and absorbed water molecules.[24] In addition, the FT-IR band at around 1630 cm^{-1} in the N-doped and pure TiO_2 samples correspond to O–H stretching and bending vibrations,[28,29] and these absorbed OH groups and water molecules play significant roles in photocatalytic activity because they act as oxidizers to decompose organic pollutants.[16]

The nitrogen adsorption–desorption isotherms and BJH pore-size distribution curves of 3DOM N-TiO_2, N-TiO_2 and pure TiO_2 nanoparticles are shown in Fig. 6. It can be seen in Fig. 6a the N-TiO_2 and pure TiO_2 nanoparticles exhibit type-IV isotherms, according to IUPAC classification,[14] suggesting the presence of a mesoporous structure in the two samples. It also can be observed that a clear adsorption hysteresis loop at $0.54 < P/P_o < 0.99$ was observed in the isotherms of N-TiO_2 and pure TiO_2 samples, which could be classified as a type-H3 hysteresis loop, indicating the presence of slit-like pores.[13,30] However, 3DOM N-TiO_2 exhibits a type-II isotherm with a type-H4 hysteresis loop at a high relative pressure (P/P_o) range of 0.5–1.0,[31] prominently indicating the presence of a macroporous structure in this material, which is in agreement with the SEM results.

In addition, the BET surface area and BJH pore-size distribution were determined from the adsorption–desorption isotherm. Table 1 lists the measured surface areas and pore volumes of the three photocatalysts. The N-TiO_2 and pure TiO_2 nanoparticles show higher surface areas with the values of 59.70 and 74.20 $m^2\ g^{-1}$, respectively. Moreover, it can be seen from Fig. 6b that the pore-size distribution calculated by the desorption branch of isotherm for both N-TiO_2 and pure TiO_2

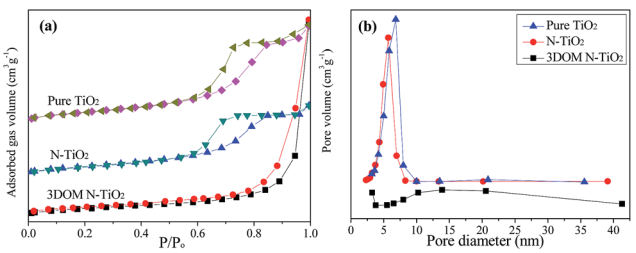

Fig. 6 (a) N_2 adsorption–desorption isotherms of all the samples; (b) corresponding pore-size distribution of all the samples.

Table 1 BET surface area, pore volume and pore size of all the prepared photocatalysts

Catalyst	S_{BET} $m^2\ g^{-1}$	Pore volume ($cm^3\ g^{-1}$)	Pore size (nm)
TiO_2	74.20	0.18	9.90
N-TiO_2	59.69	0.13	8.89
3DOM N-TiO_2	50.61	0.35	27.43

nanoparticles showed similar narrow pore-size distribution ranging from 2.32 nm to 7.98 nm, suggesting that the samples possess typical mesoporous structure. Compared with N-TiO_2 and pure TiO_2, the 3DOM N-TiO_2 sample shows relatively lower surface areas (50.61 $m^2\ g^{-1}$); however, the sample exhibits significantly higher pore volume (0.35 $cm^3\ g^{-1}$) than that of N-TiO_2 and pure TiO_2, which may be mainly attributed to the formation of 3D-interconnected macroporous networks in this solid. In addition, it should be noted that large surface areas of the as-prepared catalysts play an important role in enhancing photocatalytic activities, but they are not a decisive factor,[32] and the formation of 3DOM structure as well as the N-doping are the key factors for the enhancement of the catalytic performance of 3DOM N-TiO_2, which will be subsequently discussed.

Fig. 7 shows the UV-vis absorption spectra of 3DOM N-TiO_2, N-TiO_2 and pure TiO_2 nanoparticles. It can be observed that the pure TiO_2 exhibits photoresponsiveness in the UV region (wavelength below 395 nm) because of its wide energy band gap (3.2 eV). Compared with the pure TiO_2, a TiO_2 sample with N-doping show an apparent absorption edge in the visible-light region, particularly for the 3DOM N-TiO_2 catalyst prepared by a one-step colloidal crystal-templating method, a very broad and flat absorption tail that extends across much of the visible-light region down to 650 nm can be observed in the UV-vis absorption spectrum. This phenomenon might be caused by the following two aspects: on one hand, N species was incorporated into the lattice of TiO_2 and produced intermediate energy levels, which induced a narrow TiO_2 band gap and led to a larger and more distinct redshift in the optical absorption edge. On the other hand, the architectural structure of the photocatalyst plays a

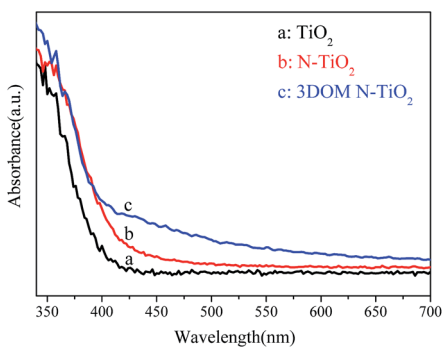

Fig. 7 UV-vis absorption spectra of pure TiO_2, N-TiO_2 and 3DOM N-TiO_2 samples.

very important role in the enhancement of optical absorption of the N-TiO_2 samples, as is well known, three-dimensionally ordered macroporous materials possess the properties of multiple scattering and slow photon effects. Thus, slow photons generated in 3DOM structures have the advantages of increasing the path length of light. Moreover, the group velocity of light significantly decreases at the edges of these wavelengths, resulting in the improvement of visible-light harvesting.[33]

The X-ray photoelectron spectroscopy (XPS) measurements were performed to test the surface chemical components and electronic sates of elements on the surfaces of N-doped TiO_2 samples. The entire XPS survey scan spectra show that both 3DOM N-TiO_2 and N-TiO_2 samples contain N, Ti, O, and C elements, which were in agreement with the EDX analysis and further confirmed the containment of N elements in the samples. Moreover, the atomic concentration of N can be calculated based on the XPS data, and the values were found to be 0.25 at% for 3DOM N-TiO_2 and 0.15 at% for N-TiO_2. In addition, the XPS spectra for the C 1s peak might be attributed to the incomplete removal of the PMMA template during calcination.

Fig. 8a shows the O 1s XPS spectra of the 3DOM N-TiO_2 and N-TiO_2. The peak at 529.7 is the characteristic of the lattice oxygen of TiO_2, and the rest of the peaks in the range of 531.0–533.3 eV can be assigned to the surface-adsorbed components of the hydroxyl group (–OH).[14,16,34] The Ti 2p XPS spectra of the 3DOM N-TiO_2 and N-TiO_2 nanoparticles are shown in Fig. 8b. Two peaks corresponding to Ti $2p_{3/2}$ and Ti $2p_{1/2}$ were observed at the binding energies of 458.5 and 464.2 eV, respectively, which can be attributed to the characteristic peaks of Ti^{4+} on the surface of N-TiO_2 catalysts.[35] There are no Ti^{3+} ions observed in the XPS spectra of the two samples. The phenomenon may be because of either the low resolution of XPS or because Ti^{3+} species exist in the subsurface or bulk.

The N 1s XPS spectra for the two samples are shown in Fig. 8c. The N 1s peak located at 397.6 eV can be assigned to N substituted at oxygen sites (substitutional N) in the TiO_2 crystal lattice to form N–Ti–N bond.[36–38] In addition, in the N 1s XPS spectra of the 3DOM N-TiO_2 catalyst, an additional peak at 399.7 eV can be attributed to interstitial N (ref. 39 and 40) atoms in the samples. It is believed that the presence of substitutional N in both the 3DOM N-TiO_2 and N-TiO_2 samples make the main contribution to the visible-light absorption and visible-light-induced photocatalytic activity.

To evaluate the photocatalytic performances of the as-prepared catalysts, the generation of hydrogen from water splitting was carried out under visible-light irradiation. As illustrated in Fig. 9, the pure TiO_2 nanoparticles show no H_2 evolution within 6 h photoreaction, which is because of the large band gap of TiO_2 and which cannot be excited by visible light. Whereas both of the two N-doped samples show significant H_2 generation activity, and the amount of hydrogen produced over N-TiO_2 with the 3DOM structure is 122.91 μmol g^{-1} under 6 h visible-light irradiation, which was higher than that of the N-TiO_2 nanoparticles (105.31 μmol g^{-1}). Thus, it can be demonstrated that the 3DOM N-TiO_2 obtained by the aforementioned method exhibit excellent properties in photocatalytic hydrogen-generation reactions.

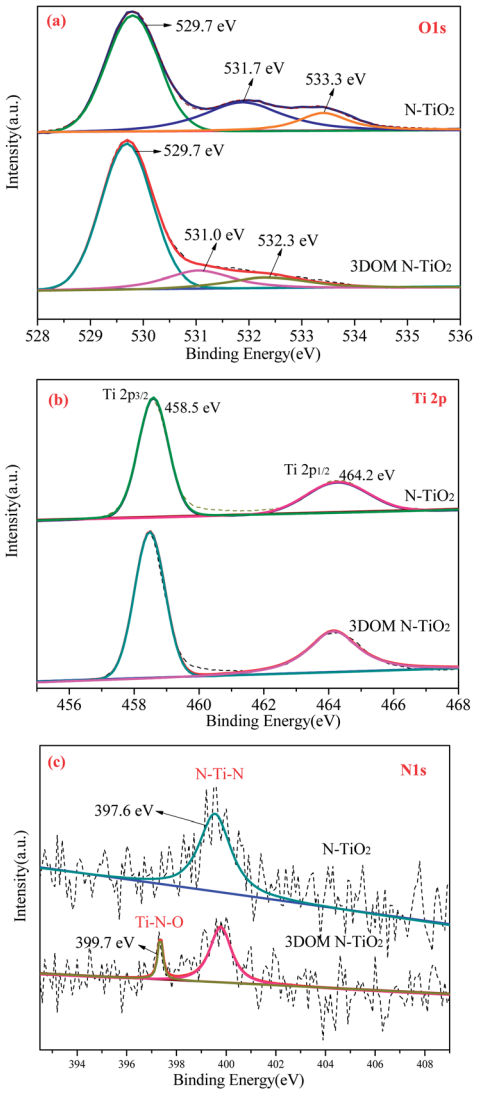

Fig. 8 XPS spectra of N-TiO_2 and 3DOM N-TiO_2 samples: (a) O 1s XPS spectra; (b) Ti 2p XPS spectra; and (c) N 1s XPS spectra.

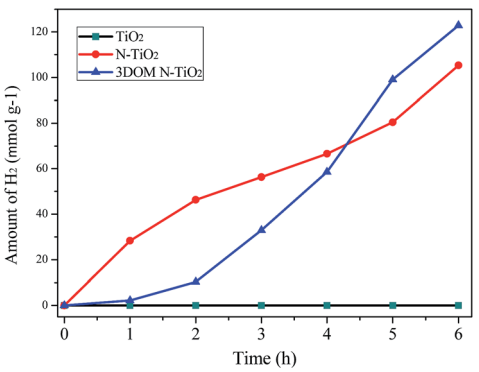

Fig. 9 Photocatalytic H_2 production efficiency over pure TiO_2, N-TiO_2 and 3DOM N-TiO_2 samples under visible-light irradiation.

In addition to the generation of H_2 from water splitting, the photocatalytic degradation of the organic pollutants was also evaluated over the as-prepared photocatalysts, and the RhB dye was chosen as the simulated pollutant. Herein, the photocatalytic activities of N-TiO_2 and pure TiO_2 nanoparticles were tested under the same condition, which was used as the reference. As shown in Fig. 10, no degradation of RhB can be observed in the absence of the photocatalyst, indicating that the RhB dye is very stable under visible-light irradiation. Moreover, pure TiO_2 nanoparticles show no visible-light-driven activity, which can be attributed to lower visible-light absorption caused by the wide energy band gap of TiO_2.[41–43] In contrast, N-TiO_2 nanoparticles and 3DOM N-TiO_2 exhibit stronger photocatalytic performance under visible-light irradiation, and the RhB degradation rate is around 76.96% and 87.16%, respectively, within a 180 min photoreaction. It can be seen that the doping of N in TiO_2 has a significant effect on the visible-light catalytic activity of titania.

In addition, the photocatalytic degradation of RhB over all the as-prepared samples was evaluated under full sunlight irradiation. As shown in Fig. 11, 3DOM N-TiO_2 and N-TiO_2 nanoparticles showed excellent photocatalytic activities compared with the pure TiO_2 nanoparticles. After 90 min photodegradation reaction, the degradation rate of RhB solution for 3DOM N-TiO_2, N-TiO_2 and pure TiO_2 nanoparticles are about 90.41%, 90.86% and 68.25%, respectively, suggesting that doping N atoms into the TiO_2 lattice not only enhanced the visible-light activity but also increased the full sunlight photocatalytic performance of the samples.

On the basis of the abovementioned discussion, it can be concluded that 3DOM N-TiO_2 and N-TiO_2 show excellent photoactivities in both photodegradation and H_2 evolution reactions. This phenomenon can be attributed to the N-doping process in our preparation. It is well known that nitrogen doping can induce the formation of an isolated band above the valence band edge of TiO_2,[22,24] which leads to a reduction in bandgap energy. Furthermore, the narrow band gap of the 3DOM N-TiO_2 favors the transfer of photogenerated electrons and results in more electrons, thereby allowing holes to participate in the photocatalytic redox reaction. Thus, N-doped TiO_2 exhibited enhanced photocatalytic activity under visible-light irradiation. In addition, it is clear that the 3DOM N-TiO_2 shows significantly higher photodegradation efficiency than the N-TiO_2 catalyst, which can be attributed to the unique 3DOM structure of the sample. It is well-known that 3DOM materials have large pore volume, periodicity and tailored pore structure, as well as exhibiting multiple scattering and slow photo effects. Therefore, 3DOM structures can not only provide more surface active sites for the adsorption of pollution molecules but also have the advantages of improving mass transfer and increasing the path length of light, both of which contribute to the enhancement of light absorption and photoreaction efficiency.[11,12] Hence, we can attempt to conclude that the obtained 3DOM N-doped TiO_2 catalysts show excellent photocatalytic activity under visible-light irradiation, owing to the synergistic effect of their unique 3DOM structure, large pore volume, high crystallization degree, N-doping system and higher charge separation.

Moreover, the stability and reusability of the 3DOM N-TiO_2 catalyst was also tested by the photodegradation of RhB under visible-light irradiation. As shown in Fig. 12, after three runs of RhB photodegradation, the N-TiO_2 with 3DOM structures still shows high photocatalytic activity, and the photodegradation efficiency reached 68.04% within 120 min of visible-light

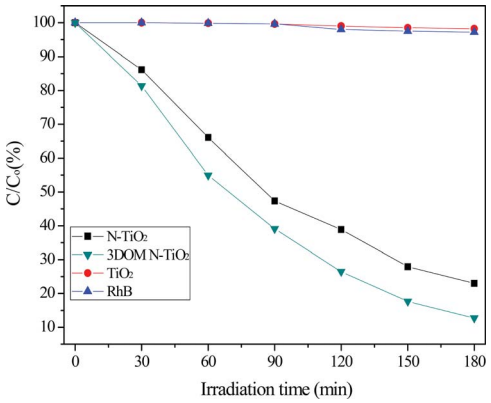

Fig. 10 Photocatalytic degradation of RhB over pure TiO_2, N-TiO_2 and 3DOM N-TiO_2 samples under visible-light irradiation.

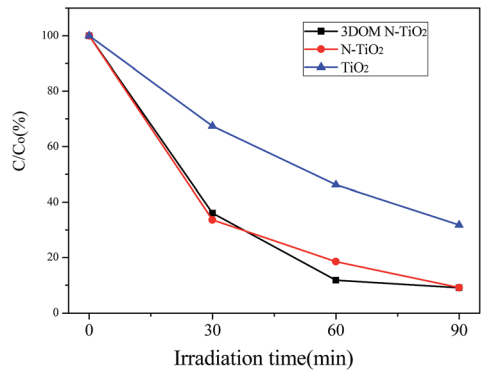

Fig. 11 Photocatalytic degradation of RhB over pure TiO_2, N-TiO_2 and 3DOM N-TiO_2 samples under full sunlight irradiation.

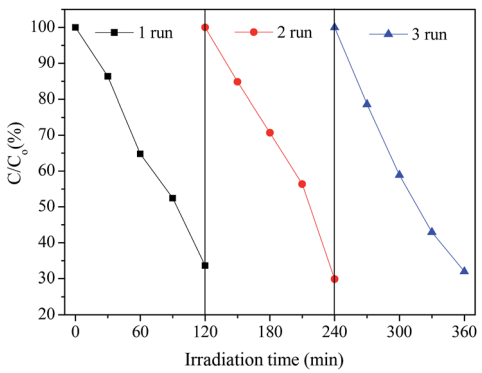

Fig. 12 Recycling tests of RhB photodegradation over 3DOM N-TiO_2 within 120 min visible-light irradiation.

illumination, which is slightly higher than that of the first round of photodegradation. The recycling test clearly revealed that the as-prepared catalysts are quite stable and possess high recyclability, which may have excellent application potentials in water treatment.

Based on the aforementioned analysis and our previous reports,[24] a possible mechanism of visible-light-driven photocatalytic activity over 3DOM N-TiO_2 was proposed and is schematically illustrated in Fig. 13. It is well-known that the doping of nitrogen in the lattice of TiO_2 could modify the electronic band structure of TiO_2, resulting in the formation of substitutional electronic states (N 2p band) on the top of the O 2p valance band, which narrows the band gap of TiO_2 and induces optical absorption into the visible-light region.[24] Hence, with the illumination of visible light, the 3DOM N-TiO_2 sample can be easily excited and produce numerous electron–hole pairs on the N 2p midgap. The photogenerated electrons are then quickly transferred to the CB of anatase TiO_2 away from the N 2p midgap state, leaving holes in the original N 2p midgap and eventually dispersing to the surface of the macroporous walls of the 3DOM photocatalysts. This process of charge transfer inhibits the recombination of electrons and holes and provides the opportunities for these charges to participate in oxidation–reduction reactions. On one hand, it is well-known that the presence of a 3DOM network within the N-doped TiO_2 sample could provide several reactive sites and allow the better diffusion of reactants (–OH, oxygen, RhB). Moreover, the interconnected macroporous network might facilitate mass transfer and lead to easy accessibility of active sites for the reactant molecules.[44] In the photoreaction, the electrons existing on the wall surface would be collected by the adsorbed O_2 to generate superoxide ($O_2^{\bullet-}$ H_2O_2). Alternatively, the two active species might produce a chemical reaction with each other to generate hydroxyl radicals ($^{\bullet}OH$) for reacting with RhB molecules and oxidizing water molecules. On the other hand, holes could not only directly oxidize RhB molecules but could also react with –OH adsorbed on the surface of the photocatalyst to generate hydroxyl radicals ($^{\bullet}OH$).[45] Therefore, it can be concluded that the 3DOM N-TiO_2 shows excellent photocatalytic activity under visible-light irradiation because of the synergistic effect of hydroxyl radicals and holes.

Moreover, except for the cooperative effect of the $^{\bullet}OH$ and holes, RhB can be photosensitized and produce electrons under visible-light illumination,[42] which favors the enhancement of the photocatalytic activity. As shown in Fig. 13, the photogenerated electrons on the LUMO level of the photoexcited RhB dye can easily and rapidly transfer to the CB of TiO_2. Moreover, because of the presence of superoxide radical ($^{\bullet}O_2^-$), RhB dye could be transformed into the cationic dye radical ($RhB^{\bullet+}$), which can be degraded into intermediate products and eventually decomposed into CO_2 and H_2O. However, because the superoxide radical ($^{\bullet}O_2^-$) could react with hydrogen peroxide (H_2O_2), the photosensitization of RhB previously described was not the key factor for the enhanced photocatalytic activity.[14]

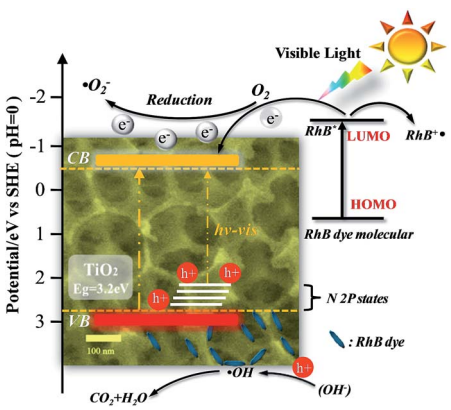

Fig. 13 Scheme illustrating the principle of charge transfer and the photocatalytic processes on the interface of the 3DOM N-TiO_2 under visible-light irradiation.

Conclusions

N-doped TiO_2 with a three-dimensionally ordered macroporous structure was successfully fabricated by a one-step colloidal crystal-template method using ethanediamine as the nitrogen source. The results show that the N species have been doped in a TiO_2 lattice, and the formation of the N 2p intermediate energy levels in the band gap leads to the enhanced visible-light absorption of 3DOM N-TiO_2. In addition, the obtained sample shows excellent photocatalytic activity for the degradation of RhB and the generation of H_2 under visible-light irradiation, which can be attributed to the synergetic effect of uniform three-dimensionally ordered macroporous structures, N-doping and stronger visible-light absorption.

Acknowledgements

This work was financially supported by the National Natural Science Foundation of China (Grant no. 21303130), the Fundamental Research Funds for the Central Universities and Natural Science Basic Research Plan in Shaanxi Province of China (Grant no. 2014JQ2066).

Notes and references

1 Z. Wang, N. S. Ergang, M. A. Al-Daous and A. Stein, *Chem. Mater.*, 2005, **17**, 6805–6813.
2 F. Cheng, Z. Tao, J. Liang and J. Chen, *Chem. Mater.*, 2008, **20**, 667–681.
3 K. T. Lee and J. Cho, *Nano Today*, 2011, **6**, 28–41.
4 R. C. Schroden, C. F. Blanford, B. J. Melde, B. J. S. Johnson and A. Stein, *Chem. Mater.*, 2001, **13**, 1074–1081.
5 S. Madhavi, C. Ferraris and T. White, *J. Solid State Chem.*, 2006, **179**, 866–872.
6 J. E. G. J. Wijnhoven and W. L. Vos, *Science*, 1998, **281**, 802–804.
7 Y. Chen, Y. Zhu and Z. Chen, *Thin Solid Films*, 2013, **539**, 122–126.
8 M. Sawangphruk and J. Limtrakul, *Mater. Lett.*, 2012, **68**, 230–233.
9 Y. Wei, Z. Zhao, T. Li, J. Liu, A. Duan and G. Jiang, *Appl. Catal., B*, 2014, **146**, 57–70.

10 S. Chai, G. Zhao, Y. Wang, Y.-N. Zhang, Y. Wang, Y. Jin and X. Huang, *Appl. Catal., B*, 2014, **147**, 275–286.
11 M. Wu, Y. Li, Z. Deng and B.-L. Su, *ChemSusChem*, 2011, **4**, 1481–1488.
12 J. I. L. Chen, G. von Freymann, S. Y. Choi, V. Kitaev and G. A. Ozin, *Adv. Mater.*, 2006, **18**, 1915–1919.
13 G. Yang, B. Yang, T. Xiao and Z. Yan, *Appl. Surf. Sci.*, 2013, **283**, 402–410.
14 C. Xue, T. Wang, G. Yang, B. Yang and S. Ding, *J. Mater. Chem. A*, 2014, **2**, 7674–7679.
15 Y. Cao, T. He, L. Zhao, E. Wang, W. Yang and Y. Cao, *J. Phys. Chem. C*, 2009, **113**, 18121–18124.
16 G. Yang, Z. Yan and T. Xiao, *Appl. Surf. Sci.*, 2012, **258**, 4016–4022.
17 G. Yang, T. Wang, B. Yang, Z. Yan and S. Ding, *Appl. Surf. Sci.*, 2013, **287**, 135–142.
18 S. C. Hayden, N. K. Allam and M. A. El-Sayed, *J. Am. Chem. Soc.*, 2010, **132**, 14406–14408.
19 G. Yang, Z. Yan and T. Xiao, *Appl. Surf. Sci.*, 2012, **258**, 8704–8712.
20 Y. Liu, L. Zhou, Y. Hu, C. Guo, H. Qian, F. Zhang and X. W. Lou, *J. Mater. Chem.*, 2011, **21**, 18359–18364.
21 Y. Ao, J. Xu, S. Zhang and D. Fu, *Appl. Surf. Sci.*, 2010, **256**, 2754–2758.
22 J. Geng, D. Yang, J. Zhu, D. Chen and Z. Jiang, *Mater. Res. Bull.*, 2009, **44**, 146–150.
23 M. M. Joshi, N. K. Labhsetwar, P. A. Mangrulkar, S. N. Tijare, S. P. Kamle and S. S. Rayalu, *Appl. Catal., A*, 2009, **357**, 26–33.
24 G. Yang, Z. Jiang, H. Shi, T. Xiao and Z. Yan, *J. Mater. Chem.*, 2010, **20**, 5301–5309.
25 R. C. Schroden, M. Al-Daous, C. F. Blanford and A. Stein, *Chem. Mater.*, 2002, **14**, 3305–3315.
26 Q. Li and J. K. Shang, *J. Am. Ceram. Soc.*, 2008, **91**, 660–663.
27 Y. Ao, J. Xu, D. Fu and C. Yuan, *J. Hazard. Mater.*, 2009, **167**, 413–417.
28 K. L. Yeung, S. T. Yau, A. J. Maira, J. M. Coronado, J. Soria and P. L. Yue, *J. Catal.*, 2003, **219**, 107–116.
29 Y. Huo, Y. Jin, J. Zhu and H. Li, *Appl. Catal., B*, 2009, **89**, 543–550.
30 J. Zhang, Y. Wang, J. Jin, J. Zhang, Z. Lin, F. Huang and J. Yu, *ACS Appl. Mater. Interfaces*, 2013, **5**, 10317–10324.
31 B. Brunauer, L. S. Deming, W. S. Deming and E. J. Teller, *J. Am. Chem. Soc.*, 1940, **62**, 1723.
32 J. Yu and L. Qi, *J. Hazard. Mater.*, 2009, **169**, 221–227.
33 P. G. O'Brien, N. P. Kherani, S. Zukotynski, G. A. Ozin, E. Vekris, N. Tetreault, A. Chutinan, S. John, A. Mihi and H. Míguez, *Adv. Mater.*, 2007, **19**, 4177–4182.
34 Y. C. Zhang, J. Li and H. Y. Hu, *Appl. Catal., B*, 2012, **123**, 20.
35 K. Yu, S. Yang, H. He, C. Sun, C. Gu and Y. Ju, *J. Phys. Chem. A*, 2009, **113**, 10024–10032.
36 J. Wang, W. Zhu, Y. Zhang and S. Liu, *J. Phys. Chem. C*, 2007, **111**, 1010.
37 Y. Sheng, Y. Xu, D. Jiang, L. Liang, D. Wu and Y. Sun, *Int. J. Photoenergy*, 2008, **2008**, 1.
38 S. Hoang, S. Guo, N. T. Hahn, A. J. Bard and C. B. Mullins, *Nano Lett.*, 2012, **12**, 26–32.
39 X. Chen and C. Burda, *J. Am. Chem. Soc.*, 2008, **130**, 5018–5019.
40 A. Fujishima, X. T. Zhang and D. A. Tryk, *Surf. Sci. Rep.*, 2008, **63**, 515–582.
41 B. Liu, L.-M. Liu, X.-F. Lang, H.-Y. Wang, X. W. Lou and E. S. Aydil, *Energy Environ. Sci.*, 2014, **7**, 2592–2597.
42 T. Wang, G. Yang, J. Liu, B. Yang, S. Ding, Z. Yan and T. Xiao, *Appl. Surf. Sci.*, 2014, **311**, 314–323.
43 X. Xu, G. Yang, J. Liang, S. Ding, C. Tang, H. Yang, W. Yan, G. Yang and D. Yang, *J. Mater. Chem. A*, 2014, **2**, 116–122.
44 Y. Dong, Y. Wang, T. Cai, L. Kou, G. Yang and Z. Yan, *Ceram. Int.*, 2014, **40**, 11213–11219.
45 Y. Wang, W. Yang, L. Zhang, Y. Hu and X. W. Lou, *Nanoscale*, 2013, **5**, 10864–10867.